

NONUNIFORM PHOTONIC CRYSTALS FOR MULTICOLOR INFRARED PHOTODETECTION

Z. Jakšić, R. Petrović^a, Z. Djurić

IHTM – Institute of Microelectronic Technologies and Single Crystals, Njegoševa 12,
11000 Belgrade, Yugoslavia

^aInstitute of Physics, P. O. Box 57, 11001 Belgrade, Yugoslavia

It is described the application of nonuniform photonic crystals for the enhancement of infrared semiconductor photodetector operation. We designed a photonic-crystal enhanced (PCE) single-chip multicolour photodetector for (3-5) μm infrared range based on a linear semiconductor detector array monolithically integrated with a nonuniform photonic crystal filter. A wedge-shaped defect slab is introduced into the structure instead of one of the layers. The stop band coincides with the spectral sensitivity range of the photodetector array, while the defect gives a transmission peak within that range. The defect thickness varies along the array length and thus shifts the transmission peak wavelength. The peak frequency is tuned by choosing the geometrical parameters of the wedge. In our experiments, thin alternating Si and SiO_2 films were sputtered onto the array surface, thus forming a 1D variable filter structure. The defect was introduced by gradually changing the middle Si layer thickness across the array utilizing in-situ oblique deposition within the sputtering system.

(Received December 14, 2001; accepted March 4, 2002)

Keywords: Photodetectors, Infrared Imaging, Thin films, Photonic Crystals, Coatings, Multilayers

1. Introduction

Photonic crystals [1] find increasingly practical applications in optoelectronics. They may be defined as 1D, 2D or 3D artificial structures with periodically changing dielectric permittivity and a large enough permittivity contrast, causing photons to behave similar to electrons in semiconductor crystal lattices. In such a structure a photonic band gap (PBG) appears, an energy band in which electromagnetic waves are evanescent. A photonic crystal thus behaves like a high-efficiency mirror for electromagnetic radiation frequencies within the photonic band gap. In 3D structures this behaviour is independent of the angle of incidence, while for 1D and 2D photonic crystals there is a strong angular dependency in 2 planes or 1 plane, respectively.

Another feature of PBG structures are their defect modes, i.e. the allowed energy levels in photonic band gaps appearing when the symmetry of photonic crystal is broken. These levels are similar to impurity levels in semiconductor lattices [2, 3]. The lattice symmetry may be disturbed by adding high-permittivity material to the unit cell (donor, introducing a mode originating at the bottom of the conduction band) or removing it from the unit cell (acceptor, with a mode originating at the top of the valence band). The result is a sharp transmission peak on a frequency corresponding to the defect. One can tune the defect mode frequency by varying the properties of the defect, i.e. by changing its thickness or dielectric permittivity.

The use of photonic crystals for enhancement of photodetector performance (Photonic Crystal Enhancement, PCE) was proposed in [4] and elaborated in [5, 6]. A PCE photodetector is immersed within a photonic crystal with a PBG equal to or wider than the electron band gap of the semiconductor material used. A defect is introduced into the photonic crystal on the incident side with its transmission peak tuned to the desired wavelength. Thus the structure detects the narrow band

around the desired frequency and the PBG behaves as a notch-filter. A much more important consequence is that the radiative recombination is suppressed in such a structure, due to the inhibition of spontaneous radiation within the photonic crystal and the resulting augmented reabsorption [4]. The result is enhanced BLIP (Background Limited Infrared Photodetector) performance in devices in which radiative recombination is significant.

In this paper we deal with PCE using nonuniform photonic crystals [7], [8]. We define nonuniform photonic crystals as those whose lattice parameters slowly or abruptly vary with spatial coordinate. The properties which may be varied include all the geometrical parameters of the unit cell plus material type and doping levels (defect modes), i.e. all of the variables determining the macroscopic behaviour of a photonic crystal. A consequence of the nonuniformity is that the conduction, valence and impurity bands are dependent on the spatial coordinate(s). This dependence can be tailored. Nonuniform photonic crystals are thus a generalization of conventional PBG materials. An illustration of a nonuniform 2D triangular photonic crystal is shown in Fig. 1.

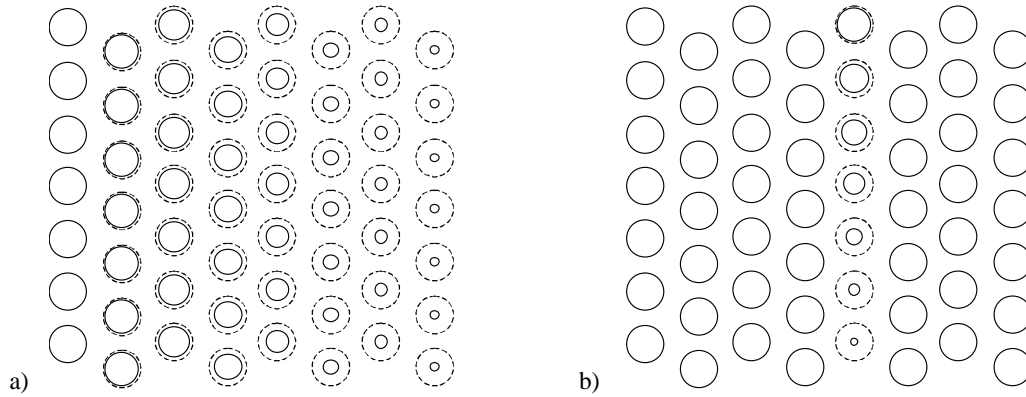


Fig. 1. Illustration of possible nonuniform 2D triangular photonic crystals. a) nonuniform lattice; b) nonuniform channel defect. Dotted lines represent isotropic (uniform) case.

Probably the most obvious way to analyse the application of photonic crystals is to use 1D structures. These are relatively easy to fabricate and the deposition methods used are well established and easy to control (production of stratified dielectric thin film structures). A defect-free 1D photonic crystal reduces to a Bragg-type distributed planar mirror. Corresponding nonuniform structures in this case are Fabry-Perot filters with a linearly variable spacer (defect) [9]. These are utilised e.g. in flatness uniformity testing [10], optical thickness measurements [11], in telecommunications as waveguide tapering Fabry-Perot cavities for wavelength demultiplexing (WDM) [12, 13], etc. Structures with a stepwise changing thickness are also used [14, 15].

In this work we apply the concept of photonic crystal enhancement of infrared photodetector arrays using variable defect 1D stacks, i.e. utilizing nonuniform photonic band gap materials. We combine this concept with another one, that of omnidirectional 1D photonic crystals [16]. This allows us to obtain in our nonuniform structures stop bands insensitive to the radiation direction. We describe a practical application of the above. We present the design procedures, including an algorithm for calculation of the PCE detector parameters. We present our experimental results and outline possible directions of future research.

2. Structure design

Basically our device consists of a 1D omnidirectional photonic crystal structure integrated with a linear photodetector array and with a defect whose thickness is continually or stepwise changing along one direction. The function of the defect can be regarded as that of a Fizeau-type

interferometric structure coupled on both sides with dielectric mirror. The radiation is normally incident to the photonic crystal surface.

The reflection of such structures shows a distinct minimum (transmission peak) within the forbidden band, at a wavelength dependent on the defect layer thickness. Since the defect thickness continually changes along the array, each its point corresponds to a transmission peak on a different wavelength. The wavelength range of a given detector element will be thus determined by the defect thickness at the beginning and at the end of the detector. In this manner the whole detector array will divide the spectral range into a number of sub-ranges equal to the number of the array elements, and each detector will “see” only the subrange corresponding to the thickness of the wedge part above it. Thus each element will receive and integrate all the wavelengths in its particular subrange (“integrator”-type structure).

In the case of a stepwise changing thickness, each detector “sees” only one constant thickness, but different from all the other elements in the array. In this manner each element receives only a very narrow peak of radiation at a given wavelength and the spectral dependence of array sensitivity will consist of a number of distinct (and equidistantly spaced) peaks (“comb” structure).

We designed our structures for the near infrared wavelength range (NWIR) (3-5) μm . We chose LN_2 -cooled indium antimonide photovoltaics as the most suitable photonic detectors for this range [16].

We chose silicon and silicon dioxide for our 1D photonic crystal filter. A detector array is integrated with the photonic crystal in the manner shown in Fig. 2.

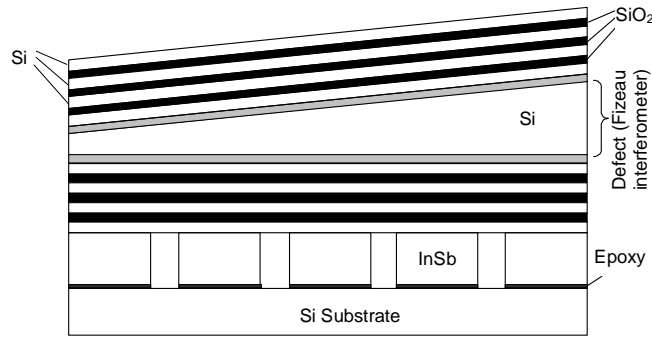


Fig. 2. Schematic presentation of a linear photodetector array enhanced by a photonic crystal with a wedge-shaped defect. The wedge slope is grossly exaggerated.

To calculate the parameters of our photonic crystal structure incorporating a defect mode, we start from the electromagnetic wave equation [9] obtained from the Maxwell's equations for a general stratified 1D medium analogous to the Kronig-Penney model [17]. We calculated the map of photonic band gaps of our structure by applying the formalism described by Joannopoulos et al [18] and obtaining the following transcendental equation [5]:

$$\cos(\kappa d) = \cos \left[2\pi \frac{d}{\lambda} \left(1 - \frac{d_1}{d} \right) n_2 \right] \cos \left[2\pi \left(\frac{d}{\lambda} \right) \left(\frac{d_1}{d} \right) n_2 \right] - \left(\frac{n_2 + n_1}{n_1 + n_2} \right) \sin \left[2\pi \left(\frac{d}{\lambda} \right) \left(1 - \frac{d_1}{d} \right) n_2 \right] \sin \left[2\pi \left(\frac{d}{\lambda} \right) \left(\frac{d_1}{d} \right) n_2 \right] \quad (1)$$

where κ is the Bloch vector (crystal momentum), d is total thickness of one layer pair, d_1 is the thickness of a stratum with high refractive index (the other stratum thickness is d_2 , so that $d = d_1 + d_2$). The corresponding refractive indexes are n_1 and n_2 . The above equation is only satisfied for those frequencies for which the right hand side is between -1 and $+1$. The frequencies that do not satisfy the condition form photonic band gaps.

We assume that the refractive indices of silicon and silicon dioxide are constant for the wavelengths (3-5) μm ($n_1 = n_{Si} = 3.46$, $n_2 = n_{SiO_2} = 1.46$) and that their absorption coefficient can be neglected in that range.

The reflection coefficient of the structure was calculated using the transfer matrix approach for the 1D case (e.g. [17, 19, 20]). To this purpose, the electric field in each homogeneous layer of our stratified structure is written as a superposition of incident ($E_j^{(i,l)}$) and reflected ($E_j^{(r,l)}$) plane waves (j denotes the number of the layer pair, $l = 1, 2$ is the number of strata within the j -th layer, r stands for the reflected and i for the incident wave). We assume the Bloch (Floquet) periodicity and apply the condition of continuity of electric and magnetic fields and their first derivatives at the layer boundaries.

The connection between the j -th and $(j-1)$ -th layer is [19]

$$\begin{bmatrix} E_j^{(i,l)} \\ E_j^{(r,l)} \end{bmatrix} = \begin{bmatrix} P_{11} & P_{12} \\ P_{21} & P_{22} \end{bmatrix} \begin{bmatrix} E_{j-1}^{(i,l)} \\ E_{j-1}^{(r,l)} \end{bmatrix} = [P] \begin{bmatrix} E_{j-1}^{(i,l)} \\ E_{j-1}^{(r,l)} \end{bmatrix} \quad (2)$$

where $[P]$ is the transfer matrix with its elements

$$\left. \begin{aligned} P_{11} &= e^{\pm ik_1 d_1} \left[\cos k_2 d_2 \pm \frac{i}{2} \left(\frac{n_2}{n_1} + \frac{n_1}{n_2} \right) \sin k_2 d_2 \right] \\ P_{12} &= e^{\pm ik_1 d_1} \left[\pm \frac{i}{2} \left(\frac{n_2}{n_1} - \frac{n_1}{n_2} \right) \sin k_2 d_2 \right] \end{aligned} \right\} k_{1,2} = \frac{2\pi}{\lambda} n_{1,2}. \quad (3)$$

For an M -layer structure we utilize the Chebyshev equality [9] to obtain

$$\begin{bmatrix} E_0^{(i,l)} \\ E_0^{(r,l)} \end{bmatrix} = \begin{bmatrix} P_{22} U_{M-1} - U_{M-2} & -P_{12} U_{M-1} \\ -P_{21} U_{M-1} & P_{11} U_{M-1} - U_{M-2} \end{bmatrix} \begin{bmatrix} E_M^{(i,l)} \\ E_M^{(r,l)} \end{bmatrix} \quad (4)$$

where $U_M = \sin[(M+1)\kappa d] / \sin(\kappa d)$ is the Chebyshev polynomial of the second kind, and the Bloch wavenumber is

$$\kappa = \frac{1}{d} \arccos \left(\frac{P_{11} + P_{12}}{2} \right). \quad (5)$$

The reflectance of the structure without a defect is [19]

$$r_M = \frac{P_{21} U_{M-1}}{P_{11} U_{M-1} - U_{M-2}}. \quad (6)$$

In the case when the refractive index of incident medium n_a is not equal to n_1 , we have [17]

$$r = \frac{\frac{|n_a - n_1|}{n_a + n_1} + r_M}{1 + \frac{|n_a - n_1|}{n_a + n_1}}. \quad (7)$$

Finally, we calculate the reflection coefficient as the squared absolute value of the Fresnel reflectance (7).

A defect is taken into account by writing the transfer matrix for the part of the photonic crystal structure from the incident surface to the defect layer (its order being $M/2$, since we replace the middle layer by the wedge defect) multiplying it from the right by the matrix corresponding to the defect thickness and finally multiplying again the whole product by the transfer matrix of the $M/2$ order. Then we calculate the reflection coefficient in the manner described above.

For continuously changing defect thickness we divided the width of the defect into infinitesimally narrow segments whose thickness may be regarded as constant and summed the contributions of all the segments over a single detector. Thus we were able to determine the total transmission per an element.

For our photonic crystal we used the calculated photonic band gap maps to choose $d = 0.9 \mu\text{m}$ and $d_1 = 0.27 \mu\text{m}$. The total number of the layer pairs (including the one with the wedge defect) was 7, starting and ending with SiO_2 layers. For such a structure we obtained the dependence of the transmission peak position on the defect thickness shown in Fig. 3. The minimum and the maximum thickness of the Si wedge determine the shortest and the longest peak wavelength.

3. Experimental

We fabricated the experimental samples of our photonic crystal structure with a wedge-shaped defect by rf diode sputtering of thin alternating Si and SiO_2 layers. The pressure before deposition was kept below 2×10^{-6} mbar. The deposition temperature was maintained below 100°C . Sputtering was performed at 1 kW rf power with circular cathode 200 mm in diameter, under Ar partial pressure of 1×10^{-2} mbar. The deposition rates were approximately 3.6 nm/min for Si and 2.8 nm/min for SiO_2 films. After deposition, the thickness of the deposited Si/ SiO_2 structure was measured by Talystep[®]. The thickness of the sputtered stacks was $0.27 \mu\text{m}$ (Si) and $0.63 \mu\text{m}$ (SiO_2). A total of 7 Si/ SiO_2 layer pairs (including the defect layer) was sputtered onto the InSb substrate.

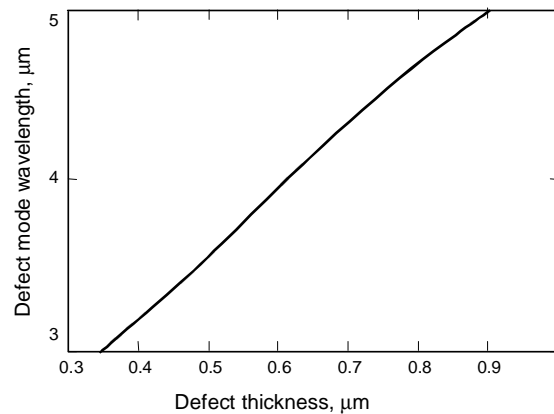


Fig. 3. The dependence of the defect mode wavelength on the defect thickness for 7-layer Si/ SiO_2 combination.

The wedge-shaped Si defect was fabricated making use of the built-in spatial inhomogeneity of the sputtered particles distribution within the growth chamber. After the conventional deposition of the first half of the stacks (three layer pairs) the wafer was placed within the system at an oblique angle and thus the deposited layer was thinner in the parts farther from the cathode. Using the known spatial distribution within the system, the tapered defect layers were tailored to obtain the desired characteristics.

The thickness of defects varied from (490-560) nm on the thinnest part to (1.00-1.35) μm on the thickest part. The length of the structures was between 20 mm and 30 mm. Thus the length of our structures along the defect slope was very large compared to the thickness of the defect (typically 0.5 to 0.9 μm) and the wedge angle slope always remained below 0.01 degrees.

After depositing the wedge-shaped defect the wafer was returned to the horizontal position and the remaining layer pairs were deposited.

Layers with constant defect thickness (600 nm), and layers without a defect were deposited in the same deposition run in order to provide control samples.

The spectral characteristics of the structures with tapering defects were measured on the Fourier Spectrometer Magna-IR Nicolet. A mean value from 50 measurements was taken. A circular light spot 5 mm in diameter was used to scan the defect along its slope and the transmission spectral curves were measured for each of its positions. The amplitude of the measured transmission at the defect peak wavelength varied from 8% to 17% among different samples. Small variations of the shape of the bands with the spot position changes were observed.

Fig. 4 shows the measured spectral transmission of a photonic crystal layer with the defect thickness linearly varying from 540 nm to 760 nm, deposited on a silicon substrate, with a circular IR radiation spot 5 mm in diameter. The comparison of the spot position with the dependence shown in Fig. 3 shows a good agreement between calculated and experimental peak positions.

We also measured the response of the InSb photovoltaics integrated with our wedge-shaped defect 1D structures. Our InSb detectors were LN₂-cooled photodiodes fabricated by liquid phase epitaxy, active area 0.65 mm², utilizing the Moss-Burstein effect in the n⁺-region to form a self-filtering layer. The spectral responsivity of the detector elements was very flat in the (3.5 to 4.8) μm range, varying ±4%.

The infrared source was blackbody simulator Barnes 11-210 with an aperture 3.3×10^{-1} cm². The signal from the detector was led to an impedance-matching amplifier and further to the lock-in amplifier Ortholoc SC-9505. The blackbody temperature was held at 500 K. We measured on the detector elements an increasing signal changing from 150 μV to 160 μV for the wedge-defect thickness varying from 550 nm to 660 nm. This is consistent with the measured uniform relative response data for our InSb photovoltaics.

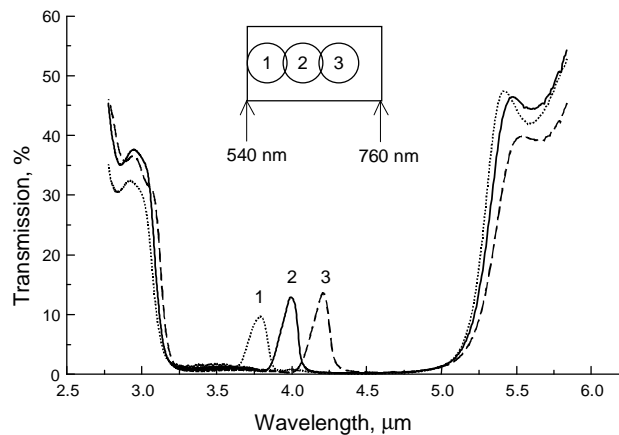


Fig. 4. Experimental dependence of transmission peaks for three different positions along the photonic band gap structure with a wedge-shaped defect; the shape of the peaks is a consequence of the circular geometry of the light spot. The inset shows the spatial position of the light spot on the wafer surface with corresponding peak numbers. The minimum and the maximum defect thickness are also indicated.

4. Spectrally sensitive matrices

Further we describe a modification of our approach in order to apply 1D photonic crystal structures with anisotropic defects for the case of focal plane arrays (and generally detector matrices). The photonic crystal defect mode thickness should in this case vary in two dimensions.

Fig. 5 shows two possible solutions to the problem. Both of them utilize chemical etching of the defect immediately after its deposition, i.e. before the rest of the structure layers is fabricated.

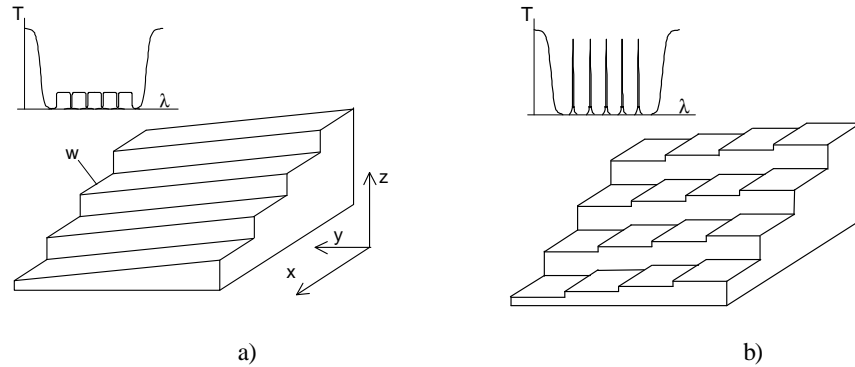


Fig. 5. Micromachined defect structures for 2D multispectral detector arrays. Insets in above left corners show general appearance of transmission characteristics (in arbitrary units); a) “integrator” type with continual variation of defect thickness; b) “comb” type, with step-changing thickness.

In Fig. 5a a tapered Si defect is processed by photolithography and wet chemical etching to obtain recessed surfaces in a manner similar to that proposed by Ünlü et al [14] but only along one dimension. After the sputtered defect is immersed in etchant normally to the direction of the slope it is then pulled out of it for the length w (equal to the detector element width) until the desired thickness is etched away. The defect is then pulled out for another stretch w and the process is repeated until the structure is finished. Each etching cycle removes a thickness equal to the height of the wedge minus its parallelepiped basis height.

For matrices with a resolution of 256 IR “colours” and square detector elements, a total of 8 steps is necessary. The largest etched thickness after all the photolithographic steps are finished remains below $0.5 \mu\text{m}$ (in each cycle only several tens of nanometers are removed from the defect), so that the structure may be regarded as quasi-planar.

The defect in Fig. 5b is obtained using the same approach, but starting from a constant-thickness defect, and repeating twice the whole procedure described above, the second time after a 90° rotation of the structure. The number of necessary steps is twice that used in the continuous case.

Fig. 6 presents an expanded view of a 1D photonic crystal-enhanced IR photodetector configuration with a built-in donor-type defect whose thickness varies along 2 axes.

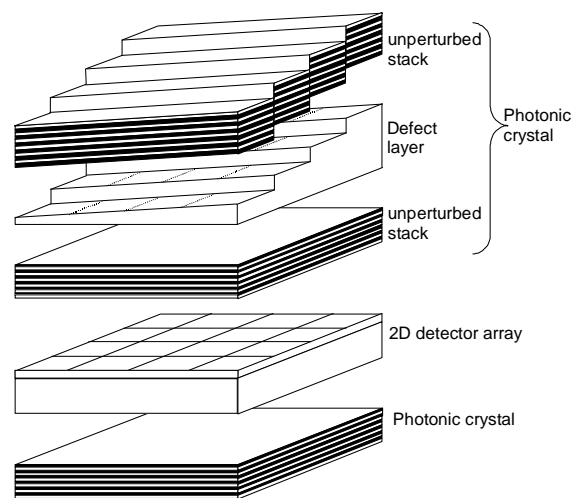


Fig. 6. Expanded view of a multispectral infrared detector chip utilizing 2D detector array and nonuniform photonic crystal filter.

Photonic crystal enhancement of detector characteristics is especially convenient for semiconductor photonic detectors, but thermal arrays could be used as well. In that case, additional

bandpass filters would be necessary to limit the detector matrix spectral range to that covered by the photonic crystal structure.

5. Conclusions

In this work we describe the enhancement of photodetector capability by utilizing nonuniform photonic crystals. The concept is applied to a 1D structure, but is valid in 2D and 3D cases. The controlled spatial inhomogeneity of the built-in defect is utilized in spectrally sensitive detection. To this purpose an InSb detector array for the spectral range 3-5 μm is integrated with the filter. The obtained structure can be used for simple spectrometric applications, but can be further refined by the application of different types of detectors.

The devices improved by nonuniform photonic crystals could perform functions of most known types of interferometers, but monolithically integrated. They may be used for multicolour detectors or spectrophotometers/monochromators on a chip. A simple recalculation of the nonuniform PCE structures in the manner described above allows us to use in it any other wavelength range, including the transmission windows utilized in optical telecommunications. Various specialized optical filters for image processing purposes could also be designed in the same manner. Some other applications could include 3D PBG diffractive optical elements, graded optical resonators, as well as other components for photonics and optoelectronics.

References

- [1] E. Yablonovitch, *Phys. Rev. Letters*, **58**, 2059 (1987).
- [2] D. R. Smith, R. Dalichaouch, N. Kroll, S. Schultz, S. L. McCall, P. M. Platzman, *J. Opt. Soc. Am. B* **10**, 314 (1993).
- [3] E. Yablonovitch, T. J. Gmitter, R. D. Meade, A. M. Rappe, K. D. Brommer, J. D. Joannopoulos, *Phys. Rev. Lett.*, **67**, 3380 (1991).
- [4] Z. Djurić, Z. Jakšić, D. Randjelović, T. Danković, *Proc. XLI Yugoslav Conf. ETRAN, Zlatibor, Serbia, June 3-6*, **4**, 121 (1997).
- [5] Z. Djurić, R. Petrović, D. Randjelović, T. Danković, Z. Jakšić, W. Ehrfeld, G. Feiertag, H. Freimuth, *Proc. 21st International Conference on Microelectronics MIEL 97, Niš, Serbia, 14-17 September*, **1**, 99 (1997).
- [6] Z. Djurić, Z. Jakšić, D. Randjelović, T. Danković, W. Ehrfeld, A. Schmidt, *Infrared Physics & Technology*, **40**, 25 (1999).
- [7] P. St. J. Russell, T. A. Birks, *J. Lightwave Tech.* **17**, 1982 (1999).
- [8] Z. Jakšić, R. Petrović, D. Randjelović, T. Danković, Z. Djurić, W. Ehrfeld, A. Schmidt, K. Hecker, *SPIE Proc.* **3680**, 611, (1999).
- [9] R. I. Seddon, B. L. Swaby, R. J. Ryll, S. E. Solberg, E. W. Anthon, "Monolithic linear variable filter and method of manufacture", *US Patent* 5, 872, 655, 1999.
- [10] M. Born, E. Wolf, *Principles of Optics*, Pergamon Press, Cambridge, 1965.
- [11] F. Pedrotti, L. Pedrotti, *Introduction to Optics*, Prentice-Hall, New York, 1987.
- [12] B. Pezeshki, F. K. Tong, J. A. Kash, D. W. Kisker, R. M. Potemski, *IEEE Phot. Tech. Lett.* **5**, 1082 (1993).
- [13] B. Pezeshki, F. F. Tong, J. A. Kash, D. W. Kisker, *J. Lightwave Tech.* **12**, 1791 (1994).
- [14] M. S. Ünlü, K. Kishino, J. I. Chyi, J. Reed, L. Arsenault, H. Morkoç, *Electronics Lett.* **26**, 1857 (1990).
- [15] M. S. Ünlü, S. Strite, *J. Appl. Phys.* **78**, 607 (1995).
- [16] D. N. Chigrin, A. V. Lavrinenko, D. A. Yarotsky, S. V. Gaponenko, *J. Lightwave Tech.* **17**, 2018, (1999).
- [17] A. Yariv, P. Yeh, *Optical Waves in Crystals*, John Wiley, New York (1984).
- [18] J. Joannopoulos, R. Meade, J. Winn, *Photonic Crystals: Molding the Flow of Light*, Princeton University Press, Princeton (1995).
- [19] P. Yeh, A. Yariv, C-S. Hong, *J. Opt. Soc. Am.*, **67**, 423 (1977).
- [20] S. S. Murtaza, M. A. Parent, J. C. Bean, J. C. Campbell, *Appl. Opt.* **35**, 2054 (1996).